

Study of η and η' photoproduction at MAMI

V. L. Kashevarov,^{1,2} P. Ott,¹ S. Prakhov,^{1,3,4} P. Adlarson,¹ F. Afzal,⁵ Z. Ahmed,⁶ C. S. Akondi,⁷ J. R. M. Annand,⁸ H. J. Arends,¹ R. Beck,⁵ A. Braghieri,⁹ W. J. Briscoe,³ F. Cividini,¹ R. Codling,⁸ C. Collicott,^{10,11} S. Costanza,^{9,12} A. Denig,¹ E. J. Downie,^{1,3} M. Dieterle,¹³ M. I. Ferretti Bondy,¹ L. V. Fil'kov,² A. Fix,¹⁴ S. Gardner,⁸ S. Gani,¹³ D. I. Glazier,^{8,15} D. Glowa,¹⁵ W. Gradl,¹ G. Gurevich,¹⁶ D. J. Hamilton,⁸ D. Hornidge,¹⁷ D. Howdle,⁸ G. M. Huber,⁶ A. Käser,¹³ S. Kay,¹⁵ I. Keshelashvili,¹³ R. Kondratiev,¹⁶ M. Korolija,¹⁸ B. Krusche,¹³ J. Linturi,¹ V. Lisin,² K. Livingston,⁸ I. J. D. MacGregor,⁸ R. MacRae,⁸ J. Mancell,⁸ D. M. Manley,⁷ P. P. Martel,^{1,17} J. C. McGeorge,⁸ E. McNicol,⁸ D. G. Middleton,^{1,17} R. Miskimen,¹⁹ E. Mornacchi,¹ C. Mullen,⁸ A. Mushkarenkov,^{9,19} A. Neiser,¹ M. Oberle,¹³ M. Ostrick,^{1,*} P. B. Otte,¹ B. Oussena,^{1,3} D. Paudyal,⁶ P. Pedroni,⁹ V. V. Polyanski,² A. Rajabi,¹⁹ G. Reicherz,²⁰ J. Robinson,⁸ G. Rosner,⁸ T. Rostomyan,¹³ A. Sarty,¹¹ D. M. Schott,³ S. Schumann,¹ C. Sfienti,¹ V. Sokhoyan,^{1,3} K. Spieker,⁵ O. Steffen,¹ B. Strandberg,⁸ I. I. Strakovsky,³ Th. Strub,¹³ I. Supek,¹⁸ M. F. Taragin,³ A. Thiel,⁵ M. Thiel,¹ L. Tiator,¹ A. Thomas,¹ M. Unverzagt,¹ S. Wagner,¹ D. P. Watts,¹⁵ D. Werthmüller,^{8,13} J. Wettig,¹ L. Witthauer,¹³ M. Wolfes,¹ R. L. Workman,³ and L. Zana¹⁵

(A2 Collaboration at MAMI)

¹*Institut für Kernphysik, Johannes Gutenberg-Universität Mainz, D-55099 Mainz, Germany*

²*Lebedev Physical Institute, 119991 Moscow, Russia*

³*The George Washington University, Washington, DC 20052-0001, USA*

⁴*University of California Los Angeles, Los Angeles, California 90095-1547, USA*

⁵*Helmholtz-Institut für Strahlen- und Kernphysik, Universität Bonn, D-53115 Bonn, Germany*

⁶*University of Regina, Regina, Saskatchewan S4S 0A2, Canada*

⁷*Kent State University, Kent, Ohio 44242-0001, USA*

⁸*SUPA School of Physics and Astronomy, University of Glasgow, Glasgow G12 8QQ, United Kingdom*

⁹*INFN Sezione di Pavia, I-27100 Pavia, Italy*

¹⁰*Dalhousie University, Halifax, Nova Scotia B3H 4R2, Canada*

¹¹*Department of Astronomy and Physics, Saint Marys University, Halifax, Nova Scotia B3H 3C3, Canada*

¹²*Dipartimento di Fisica, Università di Pavia, I-27100 Pavia, Italy*

¹³*Departement für Physik, Universität Basel, CH-4056 Basel, Switzerland*

¹⁴*Laboratory of Mathematical Physics, Tomsk Polytechnic University, 634034 Tomsk, Russia*

¹⁵*SUPA School of Physics, University of Edinburgh, Edinburgh EH9 3JZ, United Kingdom*

¹⁶*Institute for Nuclear Research, 125047 Moscow, Russia*

¹⁷*Mount Allison University, Sackville, New Brunswick E4L 1E6, Canada*

¹⁸*Rudjer Boskovic Institute, HR-10000 Zagreb, Croatia*

¹⁹*University of Massachusetts, Amherst, Massachusetts 01003, USA*

²⁰*Institut für Experimentalphysik, Ruhr-Universität, D-44780 Bochum, Germany*

(Dated: January 18, 2017)

The reactions $\gamma p \rightarrow \eta p$ and $\gamma p \rightarrow \eta' p$ have been measured from their thresholds up to the center-of-mass energy $W = 1.96$ GeV with the tagged-photon facilities at the Mainz Microtron, MAMI. Differential cross sections were obtained with unprecedented accuracy, providing fine energy binning and full production-angle coverage. A strong cusp is observed in the total cross section and excitation functions for η photoproduction at the energies in vicinity of the η' threshold, $W = 1896$ MeV ($E_\gamma = 1447$ MeV). This behavior is explained in a revised η MAID isobar model by a significant branching of the $N(1895)1/2^-$ nucleon resonance to both, ηp and $\eta' p$, confirming the existence and constraining the properties of this poorly known state.

PACS numbers: 25.20.Lj, 13.60.Le, 14.20.Gk

The photo-induced production of η and η' mesons is a selective probe to study excitations of the nucleon. The η and the η' represent the isoscalar members of the fundamental pseudoscalar-meson nonet and, in contrast to the isovector π , excitations with isospin $I = 3/2$ (Δ resonances) do not decay into ηN and $\eta' N$ final states. Several single and double-spin observables of the $\gamma p \rightarrow \eta p$ reaction have recently been measured [1–6]. A review of the experimental and phenomenological progress can be found in Ref. [7]. All model calculations [8–13] agree in the dominance of the $E_{0+}(J^P = 1/2^-)$ multipole

amplitude, which is populated by the well established $N(1535)1/2^-$ and $N(1650)1/2^-$ resonances. The existence of a third $1/2^-$ nucleon resonance, however, is still under discussion. The $N(1895)1/2^-$ is presently listed by the PDG with only two stars [14]. The experimental data for η' production is much more scarce. The most recent measurements by CLAS [4, 15] and CBELSA/TAPS [5] decreased uncertainties in the $\gamma p \rightarrow \eta' p$ differential cross sections, leaving, however, the near-threshold region still unexplored. Recently, this threshold region attracted additional attention, after the first results for the beam asymmetry Σ were presented by GRAAL [16] which, although limited in statistics, could not be reproduced by any of the existing models describing η' photoproduction [17–21]. The threshold for the $\gamma p \rightarrow \eta' p$ reaction at

*ostrick@kph.uni-mainz.de

$W = 1896$ MeV is located in a mass region that plays a key role for our understanding of the nucleon spectrum. Presently, there are no well established (four stars) states between $W = 1800$ – 2100 MeV. However, there are many state candidates and an even larger number of states predicted by quark-models [22, 23] or lattice QCD [24].

This work contributes to the study of η and η' photoproduction by presenting new, high-statistics measurements of the $\gamma p \rightarrow \eta p$ and $\gamma p \rightarrow \eta' p$ differential cross sections from reaction thresholds up to $E_\gamma = 1577$ MeV ($W = 1960$ MeV). The data were obtained with a fine binning in E_γ and cover the full range of the production angles.

The experiments were conducted using the Crystal Ball (CB) [25] as a central calorimeter and TAPS [26] as a forward calorimeter. These detectors were installed at the energy-tagged bremsstrahlung-photon beam produced from the electron beam of the Mainz Microtron (MAMI) [27]. The beam photons were incident on a liquid hydrogen target located in the center of the CB. The energies of bremsstrahlung photons, E_γ , produced by the electrons in a $10 \mu\text{m}$ copper radiator, were analyzed by detecting postbremsstrahlung electrons in tagging spectrometers (taggers). The Glasgow-Mainz tagger [28] was used in the major part of the experiments. In order to tag the high-energy part of the bremsstrahlung spectrum, a dedicated end-point tagging spectrometer (EPT) [29] was used, especially designed for η' measurements.

In this letter, we present the analysis of three independent data sets from different periods of data taking. The first data set (Run-I) was taken in 2007 with the 1508-MeV electron beam and the bremsstrahlung photons analyzed by the Glasgow-Mainz tagger up to an energy of 1402 MeV. All details on the experimental resolution of the detectors and other conditions during these measurements are given in Refs. [3, 30] and references therein. In Ref. [3], the total and differential cross sections for the $\gamma p \rightarrow \eta p$ reaction were obtained by identifying the η meson via its $3\pi^0$ decay mode. This analysis was repeated with an improved cluster algorithm, better separating electromagnetic showers partially overlapping in the calorimeters. The second important neutral decay mode $\eta \rightarrow \gamma\gamma$ was analyzed as well. The second data set (Run-II) was taken in 2009 with the 1557-MeV electron beam and the bremsstrahlung photons analyzed up to 1448 MeV. The trigger conditions for this run required more than two clusters to be detected in the CB, which suppressed severely the detection of $\eta \rightarrow \gamma\gamma$ decays, and only $\eta \rightarrow 3\pi^0$ decays were reconstructed in the analysis. More details on the Run-II conditions can be found in Ref. [31]. The third data set (Run-III) was taken in 2014 with the 1604-MeV electron beam and the bremsstrahlung photons analyzed by the EPT spectrometer from 1426 MeV up to 1576 MeV. In this run, the energy of the η' production threshold was covered, and both neutral η decay modes as well as the $\eta' \rightarrow \gamma\gamma$ and $\eta' \rightarrow \pi^0\pi^0\eta \rightarrow 6\gamma$ decays were reconstructed. More details on the Run-III conditions can be found in Ref. [29].

The selection of event candidates and the reconstruction of the outgoing particles was based on the kinematic-fit technique. Details on the kinematic-fit parametrization of the detector information and resolutions are given

in Ref. [30]. The determination of the experimental acceptance for each decay mode of η and η' was based on a Monte Carlo (MC) simulation of all processes $\gamma p \rightarrow \eta^{(\prime)} p$. The generated events were propagated through a GEANT simulation of the experimental setup. To reproduce resolutions of the experimental data, the GEANT output was subject to additional smearing, thus allowing both the simulated and experimental data to be analyzed in the same way.

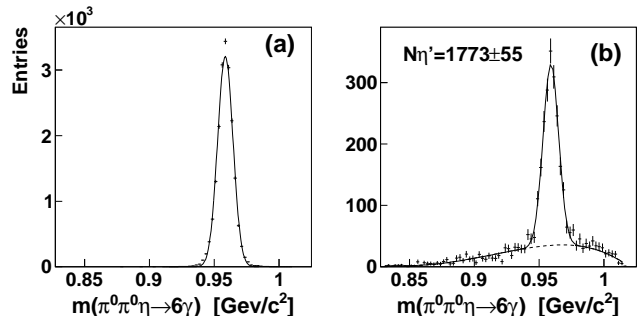


FIG. 1: $m(\pi^0\pi^0\eta \rightarrow 6\gamma)$ invariant-mass distributions obtained for $E_\gamma = 1558$ MeV and $\cos\theta = 0.1 \pm 0.01$: (a) MC simulation of $\gamma p \rightarrow \eta' p \rightarrow \pi^0\pi^0\eta p \rightarrow 6\gamma p$ with a Gaussian fit; (b) experimental spectrum fitted with the sum of a Gaussian and a polynomial of order four.

A possible background was investigated via Monte Carlo simulation of competing reactions. For both the decay modes of η' no background sources were found that could produce a peak in the $m(\gamma\gamma)$ and $m(\pi^0\pi^0\eta \rightarrow 6\gamma)$ invariant-mass distributions at the position of the η' mass. However, the selection of event candidates with the kinematic fit was not sufficient to eliminate all background in vicinity of the η' . Thus, the number of η' decays observed in every energy-angle bin was obtained by fitting experimental $m(\gamma\gamma)$ and $m(\pi^0\pi^0\eta \rightarrow 6\gamma)$ spectra with a function, describing the η' peak above a smooth background. This procedure is illustrated for one energy-angle bin in Fig. 1, showing a typical $\eta' \rightarrow \pi^0\pi^0\eta \rightarrow 6\gamma$ invariant-mass distribution and the background shape. In total, all selected events were divided into 10 $\cos\theta$ bins, where θ is the meson production angle in the c.m. frame. The covered energy range, $E_\gamma = 1447$ – 1577 MeV, was divided into 12 intervals, with the first four 6.5-MeV wide and next eight 13-MeV wide.

For the $\gamma p \rightarrow \eta p$ differential cross sections, all selected events were divided into 24 $\cos\theta$ bins. For energies below $E_\gamma = 1.25$ GeV, the present analysis of the process $\gamma p \rightarrow \eta p \rightarrow 3\pi^0 p \rightarrow 6\gamma p$ was very similar to the method described in detail in Ref. [3]. At higher energies, as in the case of η' , the background under the η decays could not be fully eliminated, and the same fitting procedure, as described above for η' , was applied.

The $\gamma p \rightarrow \eta p$ and $\gamma p \rightarrow \eta' p$ differential cross sections were obtained by taking into account the values for the corresponding η and η' branching ratios [14], the number of protons in the hydrogen target, and the photon-beam flux from the tagging facilities, corrected by the fraction rejected by the collimator. For the η cross sections, the overall systematic uncertainty due to the cal-

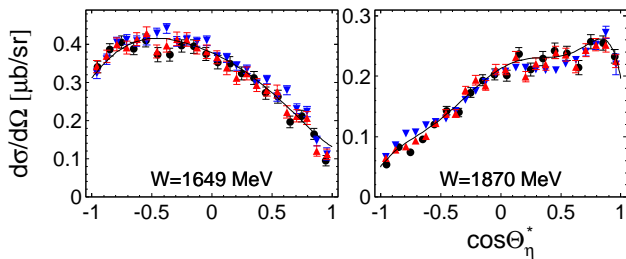


FIG. 2: (Color online) Comparison of the $\gamma p \rightarrow \eta p$ differential cross sections from Run-I (red triangles for the $\eta \rightarrow \gamma\gamma$ and blue triangles for the $\eta \rightarrow 3\pi^0$ decay mode) with the previous analysis of Ref. [3] (black circles, $\eta \rightarrow 3\pi^0$ decay) for selected energy bins. The error bars of all data points represent statistical uncertainties only. The line shows the new η MAID2016 solution discussed in the text.

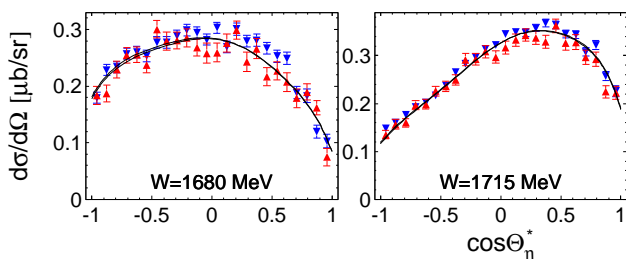


FIG. 3: (Color online) Comparison of the $\gamma p \rightarrow \eta p$ differential cross sections for Run-I (blue) and Run-II (red) in selected energy bins where the largest discrepancies are observed. The line shows the new η MAID2016 solution.

ulation of the detection efficiency and the photon-beam flux was estimated similar to our previous analyses [2, 3] as 4% for the data taken in Run-I and Run-II, and as 5% for the data taken in Run-III. Similar systematic uncertainty for the η' cross sections from Run-III is also 5%. In Fig. 2, the results from Run-I for both decay modes are compared to the previous analysis of Ref. [3]. A comparison of the differential cross sections from Run-I and Run-II for two selected energy bins, where the largest discrepancies are observed, is illustrated in Fig. 3. Finally, Fig. 4 checks Run-II against Run-III, which used a different tagging spectrometer. In general, the different data sets are in agreement within the given uncertainties. To reflect small discrepancies, which can be observed in particular regions with larger background, an additional 3% systematic uncertainty reflecting uncertainties in the angular dependence of the reconstruction efficiency was added in quadrature to all statistical uncertainties in the $\eta \rightarrow \gamma\gamma$ and $\eta \rightarrow 3\pi^0$ results of Run-I and Run-II above $E_\gamma = 1.25$ GeV, and 5% for Run III. These uncertainties were then used to combine the $\eta \rightarrow \gamma\gamma$ and $\eta \rightarrow 3\pi^0$ results together. Similar systematic uncertainties were estimated as 5% for $\eta' \rightarrow \gamma\gamma$ and 6% for $\eta' \rightarrow \pi^0\pi^0\eta \rightarrow 6\gamma$. The agreement of our $\gamma p \rightarrow \eta p$ differential cross section measurements with previous data was already demonstrated in [3]. At high energies, the results from CLAS [4] are in a better agreement with our present data than those from CBELSA/TAPS [5]. The new results for

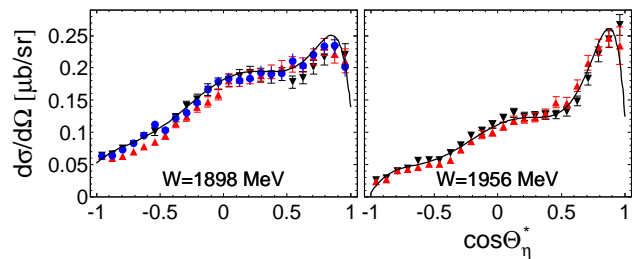


FIG. 4: (Color online) $\gamma p \rightarrow \eta p$ differential cross sections for minimal and maximal energies measured during Run-III: the black triangles ($\eta \rightarrow 2\gamma$), and red triangles ($\eta \rightarrow 3\pi^0$) were obtained in Run-III. The blue circles show results from Run-II ($\eta \rightarrow 3\pi^0$). The line shows the new η MAID2016 solution.

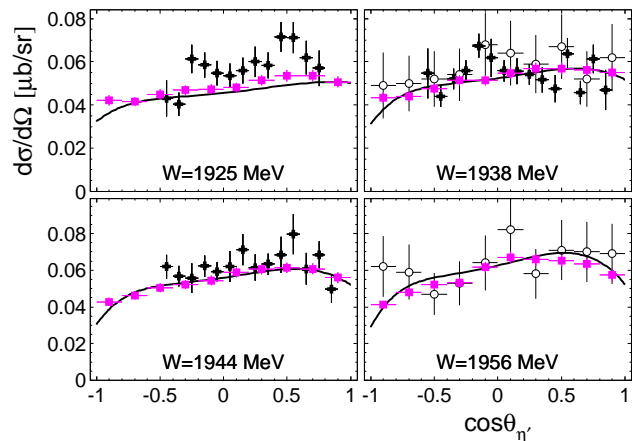


FIG. 5: (Color online) Present results for the $\gamma p \rightarrow \eta' p$ differential cross sections (magenta squares) compared to previous measurements (black crosses for CLAS [4] and black open circles for CBELSA/TAPS [5]) and to the new η MAID2016 solution (black solid line).

the $\gamma p \rightarrow \eta' p$ differential cross sections are illustrated in Fig. 5 for four energy bins which overlap with the data from CLAS [4] and CBELSA/TAPS [5]. Our results are in agreement with the previous data within the error bars, but have a much superior statistical accuracy.

The total cross sections were obtained by integrating the corresponding differential cross sections. The results obtained for the $\gamma p \rightarrow \eta p$ and $\gamma p \rightarrow \eta' p$ reactions are shown in Fig. 6 and Fig. 7, respectively. The comparison with previous data in the figures clearly demonstrates the high accuracy of our new measurements.

Besides the distinct dip at $W = 1670$ MeV [3], our new data for the $\gamma p \rightarrow \eta p$ reaction show another pronounced feature at higher energies. At the position of the η' threshold at $W = 1896$ MeV, marked by the vertical line in Fig. 6, a clear cusp is observed. The sharpness of this cusp is strongly dependent on the polar angle of the η meson, as shown in Fig. 8. While the dip at $W = 1670$ MeV is more pronounced at forward angles, the cusp effect is stronger around 90° .

One of the first dedicated models for photoproduction of η and η' mesons was the Mainz isobar model η MAID [13, 19], which was fitted to data available in

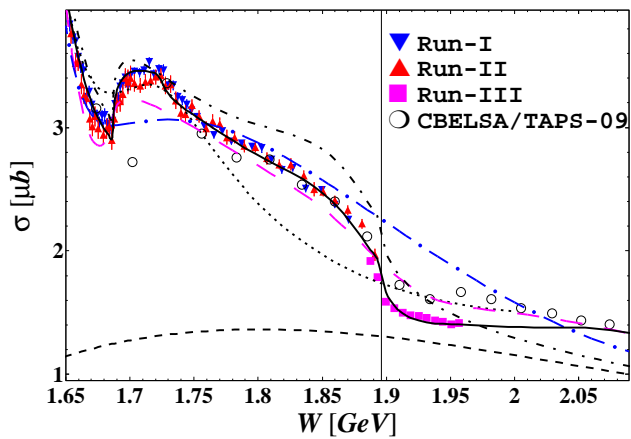


FIG. 6: (Color online) Total cross section obtained for the $\gamma p \rightarrow \eta p$ reaction along with previous measurements by CBELSA/TAPS [5]. The data are compared to the model calculations η MAID-2003 [13] (black dotted line), SAID-GE09 [9] (blue long dashed-dotted line), and BG2014-2 [8] (magenta long dashed line). The new η MAID2016 solution is shown as a black solid line. The Regge-background (dashed) as well as the sum of background and the contributions from $N1/2^-$ -resonances (dashed-dotted) are shown separately.

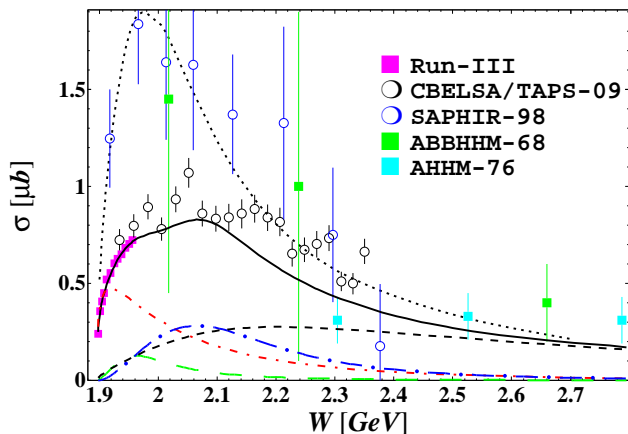


FIG. 7: (Color online) Total cross section obtained for the $\gamma p \rightarrow \eta' p$ reaction along with previous measurements by CBELSA/TAPS [5], SAPHIR [32], ABBHHM [33], and AHHM [34]. The data are compared to the model calculations η MAID-Regge-2003 [19] (black dotted line) and to the new η MAID2016 solution (black solid line). Furthermore, the background (black dashed) as well as the main resonance contributions $N(1895)1/2^-$ (red dashed-dotted), $N(1990)1/2^+$ (green long dashed), and $N(2020)3/2^-$ (blue long dashed-dotted) are shown separately.

2003. These fits are shown as dotted lines in Figs. 6 and 7, and there is no surprise that they fail to reproduce the current measurements. However, even the more recent analyses by SAID-GE09 [9] and BG2014-2 [8], are still far from agreement with the new precision data.

To interpret the new data we have developed a model based on the ideas of η MAID [13, 19]. This new η MAID2016 model includes a non-resonant background, which consists of the vector (ρ and ω) and axial-vector

TABLE I: Fit results for $J^P = 1/2^-$ resonances. Breit-Wigner parameters: mass M_{BW} , width Γ_{BW} , branching ratio to ηN channel $\beta_{\eta N} := \Gamma_{\eta N}(M_{BW})/\Gamma_{BW}$, and helicity amplitude $A_{1/2}$ in [$10^{-3}\text{GeV}^{-1/2}$]. Stars in the first column indicate an overall status of the resonance. The first row for each resonance gives a parameter set of the new η MAID solution. The second row lists the corresponding numbers given by the PDG review [14]. The parameters indicated without errors were fixed during the fit.

Resonance J^P	M_{BW} [MeV]	Γ_{BW} [MeV]	$\beta_{\eta N}$ [%]	$A_{1/2}$
N(1535)1/2 ⁻ ****	1528 ± 6	163 ± 25	41 ± 4	+115
	1535 ± 10	150 ± 25	42 ± 10	$+115 \pm 15$
N(1650)1/2 ⁻ ****	1634 ± 5	128 ± 16	28 ± 11	+45
	1655^{+15}_{-10}	140 ± 30	$14 - 22$	$+45 \pm 10$
N(1895)1/2 ⁻ **	1890^{+9}_{-23}	150 ± 57	20 ± 6	-30

(b_1) exchange in the t channel, and s -channel resonance excitations. Regge trajectories for the meson exchange in the t channel were used to provide correct asymptotic behavior at high energies. In addition to the Regge trajectories, Regge cuts with natural and un-natural parities were included according to the ideas developed in Ref. [35] for pion photoproduction. Nucleon resonances in the s channel were parameterized with Breit-Wigner shapes. The new model was fitted to data from both η and η' photoproduction on protons. In addition to the new cross sections presented in this letter, data from [1, 2, 4–6, 16] were used. A detailed publication of the model including a quantitative comparison to all available data is in preparation. Here we concentrate on the comparison to the new cross section data. A key role for the description is played by the three s -wave resonances, $N(1535)1/2^-$, $N(1650)1/2^-$, and $N(1895)1/2^-$. The importance of the first two resonances in η photoproduction is well known from previous analyses. In our model, the third resonance, $N(1895)1/2^-$, is crucial in order to describe the cusp observed in η photoproduction around $W = 1896$ MeV as well as the fast rise of the total cross section of the $\gamma p \rightarrow \eta' p$ reaction near the threshold. Presently, this resonance has only an overall two-star status according to the PDG review [14]. The present data and our analysis clearly confirm the existence of this state. We find a mass slightly below the $\eta' N$ threshold and a significant coupling to both, ηp and $\eta' p$. The parameters of all s -wave resonances are presented in Table I. As the $N(1895)1/2^-$ mass is below $\eta' N$ threshold, an effective branching ratio of $\beta_{\eta' N} = (38 \pm 20)\%$ was determined by integrating the decay spectrum above $\eta' N$ threshold according to [36]. The contributions of this and the other two important resonances, the $N(1990)1/2^+$ and the $N(2020)3/2^-$, are shown in Fig. 7.

In summary, photoproduction reactions $\gamma p \rightarrow \eta p$ and $\gamma p \rightarrow \eta' p$ have been measured from their thresholds up to the center-of-mass energy $W = 1.96$ GeV with the A2 tagged-photon facilities at the Mainz Microtron, MAMI.

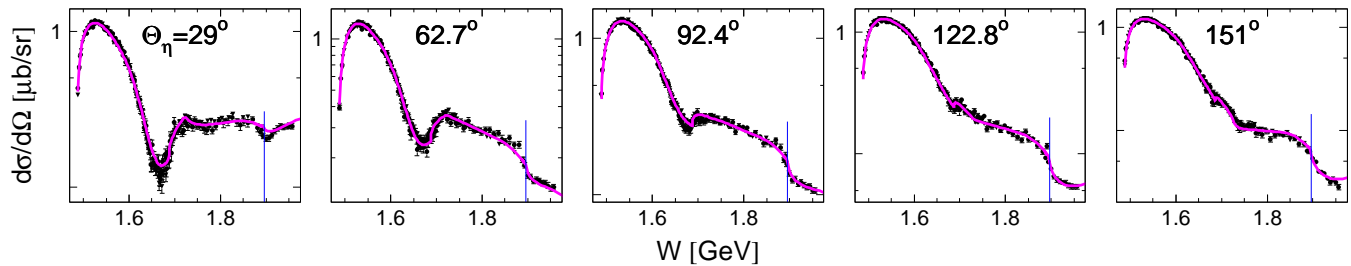


FIG. 8: (Color online) Excitation function of η photoproduction for selected angular bins. Black circles are the present data, the magenta line is the new η MAID2016 solution, the vertical line corresponds to the η' threshold.

Differential cross sections were obtained with unprecedented statistical accuracy, providing fine energy binning and full production-angle coverage. The total cross section and the excitation functions for η photoproduction demonstrate a strong cusp in the vicinity of the η' threshold, $W = 1896$ MeV. The analysis of the present data with the revised η MAID model explains such a behavior by the strong coupling of the $N(1895)1/2^-$ resonance to both channels. The new data and our analysis clearly confirm the existence of this two-star state and allow significant improvements in the determination of its parameters.

The authors wish to acknowledge the excellent sup-

port of the accelerator group of MAMI. This material is based upon work supported by the Deutsche Forschungsgemeinschaft (SFB 1044), the European Community Research Activity under the FP7 program (Hadron Physics, Contract No. 227431), Schweizerischer Nationalfonds, the UK Sciences and Technology Facilities Council (STFC 57071/1, 50727/1), the U.S. Department of Energy (Offices of Science and Nuclear Physics, Award Nos. DE-FG02-99-ER41110, DE-FG02-88ER40415, DE-FG02-01-ER41194 and DE-FG02-SC0016583) and National Science Foundation (Grant No. PHY-1039130, IIA-1358175), NSERC FRN: the MSE Program “Nauka” (Project 3.1113.2017/pp).

-
- [1] I. Senderovich *et al.*, Phys. Lett. B **755**, 64 (2016).
[2] J. Akondi *et al.*, Phys. Rev. Lett. **113**, 102001 (2014).
[3] E. F. McNicoll *et al.*, Phys. Rev. C **82**, 035208 (2010).
[4] M. Williams *et al.*, Phys. Rev. C **80**, 045213 (2009).
[5] V. Crede *et al.*, Phys. Rev. C **80**, 055202 (2009).
[6] O. Bartalini *et al.*, Eur. Phys. J. A **33**, 169 (2007).
[7] V. Krusche and C. Wilkin, Prog. Part. Nucl. Phys. **80**, 43 (2014).
[8] A. V. Anisovich, E. Klempt, V. A. Nikonov, A. V. Sarantsev, U. Thoma, Eur. Phys. J. A **47**, 153 (2011); A. V. Anisovich, R. Beck, E. Klempt, V. A. Nikonov, A. V. Sarantsev, U. Thoma, Eur. Phys. J. A **48**, 15 (2012).
[9] W. J. Briscoe, I. I. Strakovsky, and R. L. Workman, Institute of Nuclear Studies of The George Washington University Database: http://gwdac.phys.gwu.edu/analysis/pr_analysis.html.
[10] V. Shklyar, H. Lenske, U. Mosel, Phys. Rev. C **87**, 015201 (2013).
[11] H. Kamano, S. X. Nakamura, T. -S. H. Lee, T. Sato, Phys. Rev. C **88**, 035209 (2013).
[12] D. Roenchen *et al.*, Eur. Phys. J. A **51**, 70 (2015).
[13] W. -T. Chiang, S. N. Yang, L. Tiator, and D. Drechsel, Nucl. Phys. A **700**, 429 (2002).
[14] C. Patrignani *et al.*, (Particle Data Group), Chin. Phys. C **40**, 100001 (2016).
[15] M. Dugger *et al.*, Phys. Rev. Lett. **96**, 062001 (2006).
[16] P. Levi Sandri *et al.*, Eur. Phys. J. A **51**, 77 (2015).
[17] K. Nakayama and H. Haberzettl, Phys. Rev. C **73**, 045211 (2006).
[18] F. Huang, H. Haberzettl, and K. Nakayama, Phys. Rev. C **87**, 054004 (2013).
[19] W. -T. Chiang, S. N. Yang, L. Tiator, M. Vanderhaegen, and D. Drechsel, Phys. Rev. C **68**, 045202 (2003).
[20] X.-H. Zhong and Q. Zhao, Phys. Rev. C **84**, 065204 (2011).
[21] V. A. Tryaschev, Phys. Part. Nucl. Lett. **10**, 315 (2013).
[22] S. Capstick and W. Roberts, Prog. Part. Nucl. Phys. **45**, S241 (2000).
[23] M. Ronniger and B.C. Metsch Eur. Phys. J. A **47**, 162 (2011).
[24] R.G. Roberts *et al.*, Phys. Rev. D **87**, 054506 (2013).
[25] A. Starostin *et al.*, Phys. Rev. C **64**, 055205 (2001).
[26] R. Novotny, IEEE Trans. Nucl. Sci. **38**, 379 (1991); A. R. Gabler *et al.*, Nucl. Instrum. Methods Phys. Res. A **346**, 168 (1994).
[27] K. -H. Kaiser *et al.*, Nucl. Instrum. Methods Phys. Res., Sect. A **593**, 159 (2008).
[28] J. C. McGeorge *et al.*, Eur. Phys. J. A **37**, 129 (2008).
[29] P. Adlarson *et al.*, Phys. Rev. C **92**, 024617 (2015).
[30] S. Prakhov *et al.*, Phys. Rev. C **79**, 035204 (2009).
[31] P. Aguar-Bartolomé *et al.*, Phys. Rev. C **88**, 044601 (2013).
[32] R. Plotzke *et al.*, Phys. Lett. B **444**, 555 (1998).
[33] ABBHMM Collaboration, Phys. Rev. **175**, 1669 (1968).
[34] W. Struczinski *et al.*, AHHM Collaboration, Nucl. Phys. B **108**, 45 (1976).
[35] L. Donnachie, Yu. S. Kalashnikova, Phys. Rev. C **93**, 025203 (2016).
[36] J. Beringer *et al.*, (Particle Data Group), Phys. Rev. D **86**, 010001 (2012), Eq. (10) on page 1270